Phase transition in polymer derived ceramics (PDCs) and its effect on mechanical response

Chi Ma and Yan Li*

Thayer School of Engineering, Dartmouth College, Hanover, NH 03755, U.S.A

* Presenting author: yan.li@dartmouth.edu
* Corresponding author: yan.li@dartmouth.edu

Abstract

Polymer-derived ceramics (PDCs) which are fabricated through pyrolysis of preceramic polymers have attracted increasing attention due to their versatility in structure architecture design and property tailoring. Shaping at the polymer state using 3D printing allows the final ceramic products to exhibit arbitrary shapes and complex architectures that are otherwise impossible to achieve through traditional processing routes. The polymer-to-ceramic phase transition also provides additional space for mechanical property tailoring. A multiscale computational model is developed to explore the phase transition mechanisms and their correlations with processing parameters and mechanical response. Calculations in this work concern PMHS/DVB. Molecular dynamics simulations are carried out first to track the chemical reaction mechanisms and atomic structure evolution. The density of generated gas during pyrolysis is transferred to the finite element model (FEM) for coupled heat transfer and phase transition analysis. FEM calculations reveal the effect of pyrolysis temperature and heating rate on structure-level phase composition and elastic modulus. It is found that there is a threshold of pyrolysis temperature above which full ceramic phase is formed. Higher heating rate promotes ceramization and leads to higher elastic modulus. In addition, volume shrinkage is found to accelerate ceramic formation which slightly enhances material strength.

Keywords: polymer derived ceramics; phase transition; molecular dynamics simulation; finite element thermal simulation.

1. Introduction

Advanced ceramics represent a key enabling technology in aerospace, defense, power generation, and healthcare industries due to their superior properties, such as lightweight [1], high strength [2], excellent thermal stability [3] and high corrosion resistance [4]. Traditional ceramic processing technique has very little control over material geometry and does not provide enough room for property tailoring [5]. The discovery of polymer derived ceramics (PDCs) in 1960 has enabled significant technological breakthroughs in ceramic science and technology [6]. This fabrication approach, which converts preceramic polymers to ceramics through heat treatment under an inert or reacting atmosphere, opens up new opportunities for property tailoring through phase transition control [7-9]. Recently, additive manufacturing technology has enabled fabrication of preceramic polymers with complex shapes and architectures [10, 11]. Shaping at the polymer state not only avoids problems related to tool wear and brittle fracture upon finishing the ceramic component, but also provides new opportunities for geometric design which is of great importance in applications, such as customized biomedical implants, body armor, and energy storage devices, etc. Understanding the effect of key processing parameters on mechanical properties of PDCs requires in-depth

understanding of the phase transition process. Experimental characterizations, e.g. thermogravimetric analysis (TGA) [12] and infrared spectroscopy [7], can track the mass loss associated with preceramic polymer decomposition during pyrolysis. However, these approaches alone cannot directly reveal the molecular structure evolution which is an important aspect of phase transition. Scanning electron microscopy (SEM) and transmission electron microscopy (TEM) [13], which can provide detailed nano/micro structure characterization, are only available after sample pyrolysis. Computational models can address some of the underlying physics that cannot be directly captured during experiment. Molecular dynamics (MD) models have been employed to simulate the chemical reaction mechanisms and atomic structure change during pyrolysis [14, 15]. However, conclusions from MD simulations cannot be directly employed to guide the manufacturing process for tailored mechanical properties due to the large time and length scale gaps. Bernard et al. [16] proposed a diffusion-controlled kinetic model which predicts polymer-to-ceramic phase transition at the structure scale. Their prediction of polymer-to-ceramic conversion did not account for the temperature field evolution or the change of heat transfer behavior during the dynamic phase transition process. In fact, the current state phase composition and distribution will largely affect the heat transfer behavior and temperature field evolution that will ultimately determine the subsequent polymer decomposition and phase redistribution. This is because the thermal conductivity of ceramics is about ten times higher than that of polymers. The thermal conductivity of the entire material tends to increase when the polymer phase is gradually converted to the ceramic phase, leading to more intensified subsequent polymer decomposition. A computational model which finds the missing link between the atomic level structure evolution and macroscale phase composition map will promote in-depth understanding of the process physics and its relationship with material response.

In this paper, a multiscale computational model is developed to study the effect of phase transition on mechanical properties of pyrolyzed PMHS/DVB by accounting for a set of systematically varied pyrolysis parameters. Continuum-scale ceramic phase formation is predicted based on the competition between gas generation and gas diffusion in Section 3.1. The effect of heating rate and pyrolysis temperature on elastic modulus is presented in Section 3.2. The effect of volume shrinkage on ceramization is discussed in Section 3.3. The developed model, which correlates key processing parameters with mechanical properties, will reduce the time and cost in developing future PDCs with tailored mechanical properties.

2. Model description

2.1 Multiscale modeling of phase transition

2.1.1 Molecular dynamics simulation based on reaction force field

A preceramic polymer system, in which polymethylhydrosiloxane (PMHS) is crosslinked by divinylbenzene (DVB), is modeled in this work. The polymer chains with the molar mass of 1500 g/mol are first constructed and randomly packed in the simulation box while DVB molecules are bonded to different polymer chains to create the network structure. The network structure is imported to large-scale atomic/molecular massively parallel simulator (LAMMPS) to obtain system equilibrium [17, 18]. The parameters of reaction force field are selected based on the work of Kulkarni et al. [19]. Constant temperature and pressure ensemble (NPT) are utilized with a time step of 0.1 fs. The pre-pyrolysis system is equilibrated at 300 K as shown in Fig. 1(a). The pyrolysis process is simulated in MD by considering a range of pyrolysis temperatures from 873 K to 5000 K with constant heating rate of 0.1 K/fs and time step of 0.2 fs. The top surface of the simulation box is set to move freely along the vertical direction. At the height of three times of the initial box length, the temperature is set to 0.1 K

by Berendsen thermostat in order to trap the diffused gas molecules. Periodic boundary conditions are applied on the rest of the surfaces.

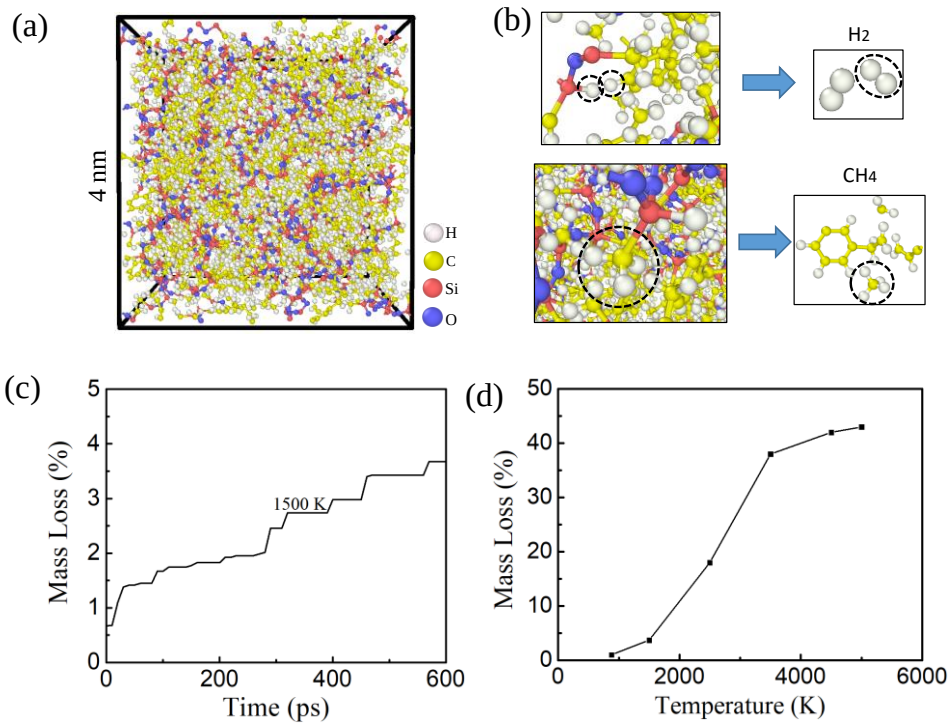

Fig. 1 (a) Equilibrated PMHS/DVB systems before pyrolysis; (b) Atomic debonding and rebonding process at 1500 K during pyrolysis; (c) Temporal evolution of mass loss at 1500 K; (d) Mass loss percentage as a function of pyrolysis temperature.

Chemical reactions during pyrolysis are elucidated in Fig. 1(b). At a pyrolysis temperature of 1500 K, bond breakage occurs to form free radicals (e.g. -CH_3) and atoms (e.g. H atoms). Gaseous products, such as H_2 and CH_4 are generated due to the new bond formation. Mass loss occurs as the gaseous products are gradually released out of the system during pyrolysis. As indicated in Fig. 1(c), the system possesses a low degree of mass loss (< 5%) when the pyrolysis temperature is 1500 K. It is noted from Fig. 1(d) that there is a steep increase of mass loss when the sample is pyrolyzed between 1500 K to 3000 K. No obvious mass loss change was observed when the pyrolysis temperature is outside this range. This conclusion agrees with the thermogravimetric analysis (TGA) [20, 21]. It should be noted that the mass loss prediction from MD cannot directly represent the experiment result at the same pyrolysis temperature. A much higher temperature is required in MD to reproduce the mass loss value from TGA [14, 22]. This is primarily due to the limited time and length scales that can be considered in current MD simulations. But the trend of mass loss as indicated in Fig. 1(d) agrees with the experimental observations. In this work, the temperature range is calibrated according to the experimental data from Li et al. [23]. The generated gas density is calculated as

$$\psi\left(T\right) = m_{\text{gas}}\left(T\right)\rho_{\text{initial}} / m_{\text{initial}}, \tag{1}$$

where $\rho_{\text{initial}} = 1.21$ g/cc and $m_{\text{gas}}\left(T\right)$ is the mass loss data from MD results. $\psi\left(T\right)$, which is the amount of generated gas per unit volume, is implemented in phase transition and heat transfer analysis in Section 2.1.2.

2.1.2 Finite element simulation of phase transition

Gaseous products, which are generated during pyrolysis, need to release out of the system so that the ceramic structure can be formed. Therefore, phase transition requires in-depth understanding of the interplay between gas generation and gas diffusion. At the structure level, a PDC sample during pyrolysis may include three phases: polymer phase (phase 1), ceramic phase (phase 2) and intermediate phase with partially decomposed polymers. Due to the huge discrepancy of thermal conductivity in each phase, non-uniform temperature field is expected when different phases coexist. Gas diffusion is triggered as a result of the gas density gradient. Gas diffusion rate $\mathrm{d}\psi/\mathrm{d}t$, is calculated as

$$\mathrm{d}\psi/\mathrm{d}t = D\sum_{i=1}^{3}\mathrm{d}\psi^2/\mathrm{d}^2x_i\,, \tag{2}$$

where D is the diffusion coefficient from the work of Merkel et al. [24]. According to the gas diffusion rate, ceramic fraction can be predicted based on the competition between gas generation and gas diffusion. At a given moment during pyrolysis, a selected volume of the sample is either under gas gain or gas loss. Ceramic formation requires $\mathrm{d}\psi/\mathrm{d}t < 0$ when gas loss is activated. The ceramic fraction φ is defined as

$$\varphi = \frac{\psi_{\text{release}}}{\psi_{\text{release}}^{\max}}\,, \tag{3}$$

where ψ_{release} is the current gas release density. $\psi_{\text{release}}^{\max}$ is the maximum gas density that can be generated in a given unit volume. Calculation of φ is carried out through a user subroutine UMATHT in ABAQUS. The finite element model in Fig. 2(a), which simulates macroscale phase transition process by accounting for both heat transfer and gas diffusion kinetics, can explicitly resolve the real-time phase composition map.

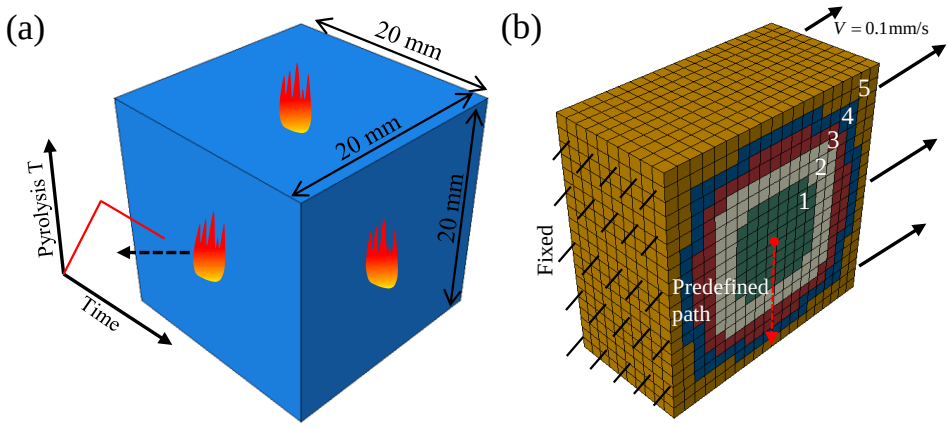

Fig. 2 (a) Scheme of the finite element model with temperature boundary conditions; (b) Schematic illustration of the phase composition map at 1600 s with pyrolysis temperature of 1273 K and heating rate of 0.63 K/s. The effective elastic modulus is extracted through the simulation of simple tension based on the given boundary and loading conditions.

2.2 Prediction of effective elastic modulus

In this study, five material regions are created based on the range of ceramic fraction φ as listed in Table 1. Fig. 2(b) illustrates the region distribution at 1600 s when the sample is pyrolyzed at 1273 K with a heating rate of 0.63 K/s. The elastic modulus at $\varphi = 0$ (pure polymer phase) and $\varphi = 1$ (pure ceramic phase) is taken as 3.7 MPa [25] and 106.8 GPa [9], respectively. It is assumed that all the regions follow isotropic linear elastic constitutive relations. The equivalent elastic modulus of each region is determined by averaging the elastic modulus of all the including phases. Simple tension simulation is carried out to extract the effective elastic modulus. The simulation prediction is compared with the analytical solution based on the Mori-Tanaka (MT) method according to Lee [26], Fisher et al. [27], Thorvaldsen [28] and Li et al. [29]. In the MT model, the effective stiffness tensor *C* is formulated as

$$C = A_0 \left[(1 - \sum_{i=1}^{N=5} f_i) C_{\text{polymer}} + \sum_{i=1}^{N=5} f_i C_i A_i^{\text{dil}} \right] , \tag{4}$$

where C_{polymer} is polymer stiffness tensor; f_i and C_i are the volume fraction and stiffness tensor of region *i*; A_0 and A_i^{dil} are the strain concentration factors following the following expressions as,

$$A_0 = \left[(1 - \sum_{i=1}^{5} f_i) I + \sum_{i=1}^{N=5} f_i A_i^{dil} \right]^{-1} \text{ and} \tag{5}$$

$$A_i^{dil} = \left[I + S_i C_{\text{polymer}}^{-1} (C_i - C_{\text{polymer}}) \right]^{-1} . \tag{6}$$

Here, I and S_i are the identity tensor and the Eshelby tensor of region *i*, respectively. Under the uniaxial tension condition in this study, only the diagonal elements of Eshelby tensors are considered. The diagonal elements can be calculated as

$$S_{diagonal} = \frac{7 - 5\nu_0}{15(1 - \nu_0)} , \tag{7}$$

with $\nu_0 = 0.48$ as Poisson's ratio of the polymer phase. The diagonal value along the *C* tensor is extracted as the effective elastic modulus. This analytical solution will be compared with the prediction from the simple tension simulation in Section 3.2.

Table 1. Region division criterion

Region number	Ceramic fraction φ
Region 1	$\varphi \leq$ 20%
Region 2	20% $< \varphi \leq$ 40%
Region 3	40% $< \varphi \leq$ 60%
Region 4	60% $< \varphi \leq$ 80%
Region 5	80% $< \varphi \leq$ 100%

3. Results and discussion

3.1 Phase distribution under different pyrolysis conditions

Macroscale phase transition simulations concern seven samples with the identical geometry as illustrated in Fig. 2(a). The pyrolysis parameters associated with each sample are listed in Table 2. In the first set of calculations, four heating rates of 0.27 K/s, 0.38 K/s, 0.63 K/s and 1.9 K/s are considered while the pyrolysis temperature is kept at 1273 K. Fig. 3 illustrates the phase distribution under each heating rate at 720 s. Fully converted ceramic phase is found at the outer layer of the sample when the heating rate is 1.9 K/s. No more fully converted ceramic phase is observed at the outer surface when the heating rate reduces to 0.63 K/s and below. Lower heating rate leads to larger undecomposed region. In the second set of calculations, heating rate is kept at 0.63 K/s, while the pyrolysis temperature of 673 K, 873 K, 1073 K and 1273 K are applied, respectively. As shown in Fig. 4, fully converted ceramic phase is observed at 1273 K when the sample is being pyrolyzed for 1600 s. In the other three samples under lower pyrolysis temperatures, no fully converted ceramic phase is observed. According to the heating history, it only takes 1227 s to reach the surface temperature of 1073 K. Further pyrolysis to 1600 s cannot help further ceramization. It can be concluded that there is a threshold of pyrolysis temperature above which full ceramic phase is formed.

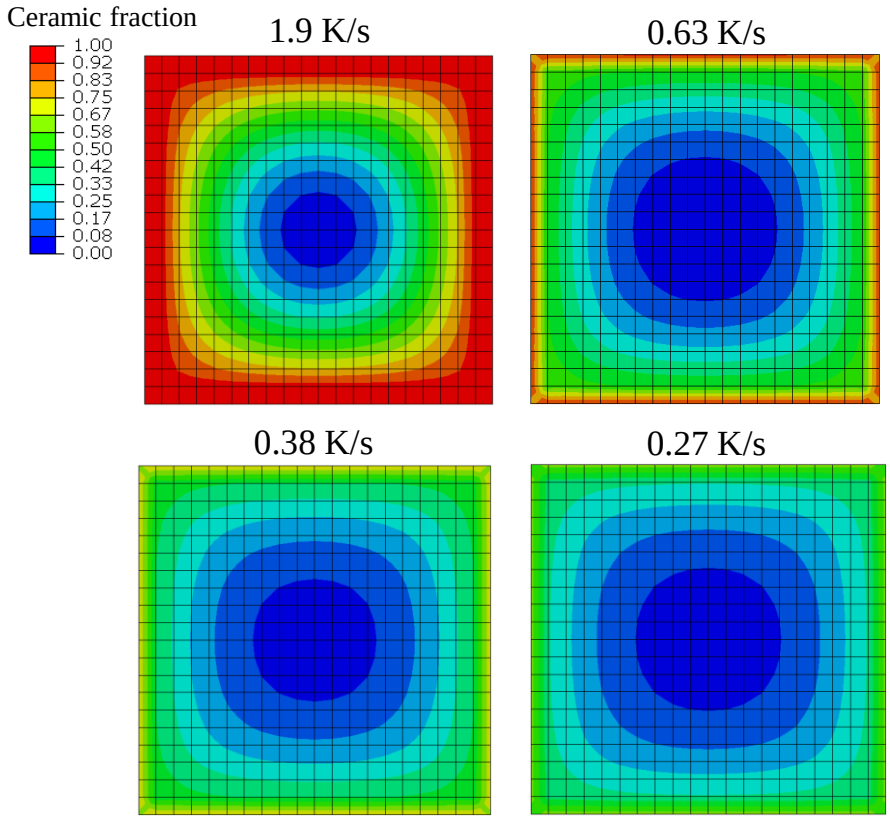

Fig. 3 Phase distribution under different heating rates at 720 s with final pyrolysis temperature of 1273 K.

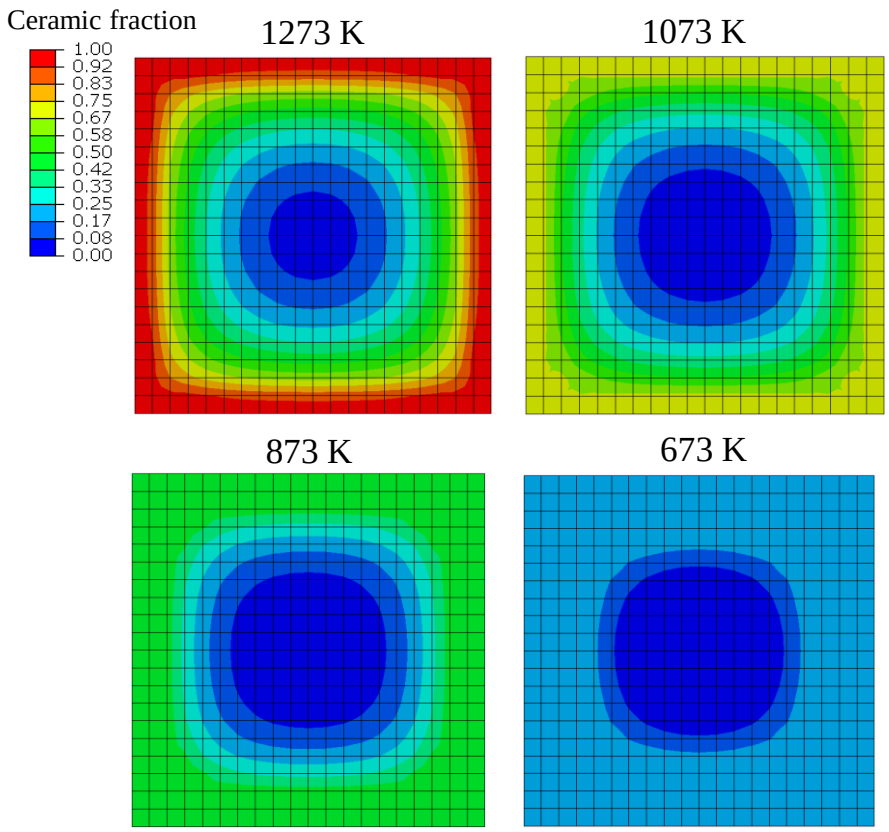

Fig. 4 Phase distribution under different pyrolysis temperature with heating rate of 0.63 K/s at 1600 s.

Table 2. Pyrolysis parameters

Sample Number	Heating rate (K/s)	Pyrolysis Temperature (K)
Sample 1	0.27	1273
Sample 2	0.38	1273
Sample 3	0.63	1273
Sample 4	1.9	1273
Sample 5	0.63	1073
Sample 6	0.63	873
Sample 7	0.63	673

3.2 Effect of pyrolysis parameters on elastic modulus

Based on the phase composition map from Fig. 3 and Fig. 4, the corresponding effective elastic modulus of each sample is predicted by both simple tension simulation and MT method as discussed in Section 2.2. As indicated in Fig. 5(b), predictions from both approaches are very close when the heating rate is below 0.63 K/s. As the heating rates increases, the discrepancy becomes larger. Overall, the MT predictions are relatively lower than the FEM predictions from the simple tension test. This trend is observed by Mortazavi et al. [30] as well. It is noticed from Fig. 5 (b) that a 41% increase of heating rate from 0.27 K/s to 0.38 K/s results in a 12% increase of elastic modulus, while a 202% increase of heating rates from 0.63 K/s to 1.9 K/s only leads to a 29% increase of elastic modulus. It can be argued that there exists an upper bond of heating rate beyond which no obvious increase of effective elastic modulus is observed at the given pyrolysis temperature. Based on the given

pyrolysis temperature range as shown in Fig. 6(b), the elastic modulus linearly increases with the pyrolysis temperature.

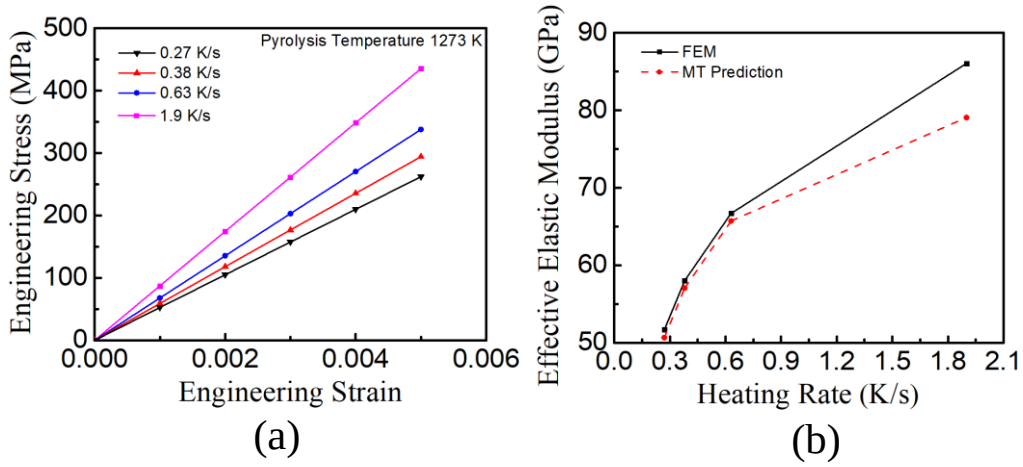

Fig. 5 (a) Effect of heating rate on engineering stress-strain behavior from simple tension simulation; (b) Comparison of effective elastic modulus as predicted from simple tension simulation and MT method at different heating rates, respectively.

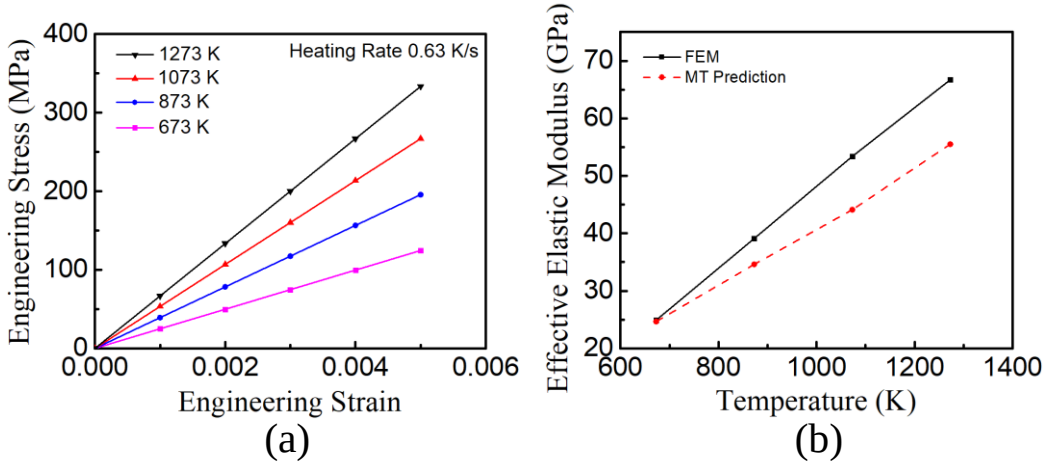

Fig. 6 (a) Effect of pyrolysis temperature on engineering stress-strain behavior from simple tension simulation; (b) Comparison of effective elastic modulus as predicted from simple tension simulation and MT method at different pyrolysis temperatures, respectively.

3.3 Effect of volume shrinkage on phase distribution and elastic modulus

Gas release during the phase transition not only leads to mass loss, but also results in volume shrinkage of the entire sample. In the following studies, we model the volume shrinkage effect by applying an equivalent hydrostatic pressure P on the sample surfaces. P is calculated according to

$$P = \frac{\Delta V}{V} \times \frac{\bar{E}}{3(1-2\bar{\nu})} \quad , \tag{8}$$

where $\bar{E}$ and $\bar{\nu}$ are the effective elastic modulus and Poisson's ratio, respectively. ΔV and V are the change of volume and initial volume of the sample, respectively.

Fig. 7 shows the effect of volume shrinkage on spatial distribution of temperature, released gas density and ceramic fraction along the pre-defined path as illustrated in Fig. 2(b). Calculations concern heating rate of 0.63 K/s and pyrolysis temperature of 1273 K. It can be inferred from Fig. 7(a) that volume shrinkage promotes heat transfer as higher temperatures are predicted along the pre-defined path. This is especially obvious towards the sample center where the normalized distance is 0. Higher temperature promotes polymer decomposition and leads to a greater amount of gas generation. On the other hand, gas diffusion which depends on the spatial gas density gradient according to eqn. (2) is also affected by the volume shrinkage. As indicated in Fig. 7(b), volume shrinkage essentially increases the gas density gradient due to the decreased spatial distance. As a result, higher ceramic fraction is expected as shown in Fig. 7(c). The effective elastic modulus predicted from the simple tension model would increase from 66.7 GPa to 72.3 GPa when the volume shrinkage effect is considered.

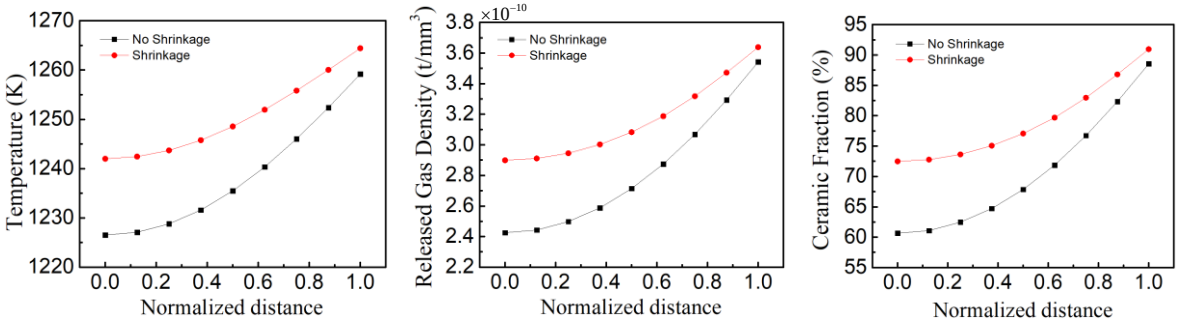

Fig. 7 Effect of volume shrinkage on spatial distribution of (a) temperature, (b) released gas density and (c) ceramic fraction at the pyrolysis temperature of 1273 K with heating rate of 0.63 K/s.

4. Summary

A multiscale computational model is developed to find the relationship among pyrolysis condition, phase transition and mechanical response. The macroscale phase distribution is determined from the interplay between gas generation and gas diffusion. Gas generation, which is associated with polymer decomposition, is calculated from the MD simulation and calibrated with the experiment data. Gas diffusion, which occurs due to the inhomogeneous temperature distribution induced gas density gradient, is analyzed through coupled heat transfer-phase transition analysis. The phase composition map, which corresponds to a given processing condition, can be explicitly extracted. The effective elastic modulus of a sample is predicted from the simple tension simulation and MT method based on its phase composition map. It is found that predictions from both approaches agree well at low heating rate and pyrolysis temperature. Volume shrinkage promotes heat transfer and ceramic formation, leading to higher prediction of effective elastic modulus. The model developed in this work will be further validated with future experiment.

Acknowledgement

The authors acknowledge the support from NH BioMade Project which is provided by the National Science Foundation's Research Infrastructure Improvement Award # 1757371, as well as the start-up funds from Thayer School of Engineering at Dartmouth College.

References

[1] M. Alizadeh-Osgouei, Y. Li, C. Wen, (2018), A comprehensive review of biodegradable synthetic polymer-ceramic composites and their manufacture for biomedical applications, Bioact Mater 4(1) 22-36.

[2] Y. Waku, N. Nakagawa, T. Wakamoto, H. Ohtsubo, K. Shimizu, Y. Kohtoku, (1997), A ductile ceramic eutectic composite with high strength at 1,873 K, Nature 389(6646) 49-52.

[3] J.F. Justin, A. Jankowiak, (2011), Ultra High Temperature Ceramics: Densification, Properties and Thermal Stability, AerospaceLab (3) p-1.

[4] T. Wei, F. Yan, J. Tian, (2005), Characterization and wear-and corrosion-resistance of microarc oxidation ceramic coatings on aluminum alloy, Journal of Alloys and Compounds 389(1-2) 169-176.

[5] J. Gonzalez Gutierrez, S. Cano, S. Schuschnigg, C. Kukla, J. Sapkota, C. Holzer, (2018), Additive manufacturing of metallic and ceramic components by the material extrusion of highly-filled polymers: A review and future perspectives, Materials 11(5) 840.

[6] P. Colombo, R. Riedel, G.D. Sorarù, H.K. Kleebe (2009), Historical review of the development of polymer derived ceramics (PDCs), Polymer Dervied Ceramics: From Nanostructure to Apllications, DEStech Publictions Inc., pp. 1-12.

[7] L. Gottardo, S. Bernard, C. Gervais, M. Weinmann, P. Miele, (2012), Study of the intermediate pyrolysis steps and mechanism identification of polymer-derived SiBCN ceramics, Journal of Materials Chemistry 22(34) 17923-17933.

[8] J. Wan, M.J. Gasch, A.K. Mukherjee, (2004), InSitu Densification Behavior in the Pyrolysis Consolidation of Amorphous Si-N-C Bulk Ceramics from Polymer Precursors, Journal of the American Ceramic Society 84(10) 2165-2169.

[9] G.D. Sorarù, L. Kundanati, B. Santhosh, N. Pugno, (2019), Influence of free carbon on the Young's modulus and hardness of polymer-derived silicon oxycarbide glasses, Journal of the American Ceramic Society 102(3) 907-913.

[10] Z.C. Eckel, C. Zhou, J.H. Martin, A.J. Jacobsen, W.B. Carter, T.A. Schaedler, (2016), Additive manufacturing of polymer-derived ceramics, Science 351(6268) 58-62.

[11] G. Konstantinou, E. Kakkava, L. Hagelüken, P.V.W. Sasikumar, J. Wang, M.G. Makowska, G. Blugan, N. Nianias, F. Marone, H. Van Swygenhoven, (2020), Additive micro-manufacturing of crack-free PDCs by two-photon polymerization of a single, low-shrinkage preceramic resin, Additive Manufacturing 35 101343.

[12] S. Venkatachalam, D. Hourlier, (2019), Heat treatment of commercial Polydimethylsiloxane PDMS precursors: Part I. Towards conversion of patternable soft gels into hard ceramics, Ceramics International 45(5) 6255-6262.

[13] S. Vry, M. Roumanie, R. Laucournet, G. Bernard-Granger, (2020), Transmission Electron Microscopy Investigations on a Polysiloxane Preceramic Polymer Pyrolyzed at High Temperature in Argon, Ceramics 3(4) 421-427.

[14] I. Ponomarev, A.C.T. Van Duin, P. Kroll, (2019), Reactive Force Field for Simulations of the Pyrolysis of Polysiloxanes into Silicon Oxycarbide Ceramics, Journal of Physical Chemistry C 123(27) 16804-16812.

[15] X. Lu, X. Wang, Q. Li, X. Huang, S. Han, G. Wang, (2015), A ReaxFF-based molecular dynamics study of the pyrolysis mechanism of polyimide, Polymer Degradation and Stability 114 72-80.

[16] S. Bernard, K. Fiaty, D. Cornu, P. Miele, P. Laurent, (2006), Kinetic modeling of the polymer-derived ceramics route: Investigation of the thermal decomposition kinetics of poly[B-(methylamino)borazine] precursors into boron nitride, Journal of Physical Chemistry B 110(18) 9048-9060.

[17] S. Plimpton, (1995), Fast parallel algorithms for short-range molecular dynamics, Journal of computational physics 117(1) 1-19.

[18] C. Ma, T. Ji, C.G. Robertson, R. Rajeshbabu, J. Zhu, Y. Dong, (2017), Molecular insight into the Mullins effect: irreversible disentanglement of polymer chains revealed by molecular dynamics simulations, Physical Chemistry Chemical Physics 19(29) 19468-19477.

[19] A.D. Kulkarni, D.G. Truhlar, S. Goverapet Srinivasan, A.C.T. Van Duin, P. Norman, T.E. Schwartzentruber, (2013), Oxygen interactions with silica surfaces: Coupled cluster and density functional investigation and the development of a new ReaxFF potential, Journal of Physical Chemistry C 117(1) 258-269.

[20] X. You, Q. Hu, X. Hu, H. Chen, W. Yang, X. Zhang, (2019), An Effective, Economical and Ultra-Fast Method for Hydrophobic Modification of NCC Using Poly (Methylhydrogen) Siloxane, Polymers 11(6) 963.

[21] R. Li, P. Hou, N. Xie, Z. Ye, X. Cheng, S.P. Shah, (2018), Design of SiO2/PMHS hybrid nanocomposite for surface treatment of cement-based materials, Cement and Concrete Composites 87 89-97.

[22] H. Gao, H. Wang, Z. Zhao, M. Niu, L. Su, Y. Wei, (2018), Reactive Dynamics Simulation Study on the Pyrolysis of Polymer Precursors to Generate Amorphous Silicon Oxycarbide Structures, Journal of Physical Chemistry C 122(10) 5767-5773.

[23] Y.J. Li, C.Y. Fan, J.P. Zhang, X.L. Wu, (2018), A promising PMHS/PEO blend polymer electrolyte for all-solid-state lithium ion batteries, Dalton transactions 47(42) 14932-14937.

[24] T.C. Merkel, V.I. Bondar, K. Nagai, B.D. Freeman, I. Pinnau, (2000), Gas sorption, diffusion, and permeation in poly (dimethylsiloxane), Journal of Polymer Science Part B: Polymer Physics 38(3) 415-434.
[25] Z. Wang, A.A. Volinsky, N.D. Gallant, (2014), Crosslinking effect on polydimethylsiloxane elastic modulus measured by custom-built compression instrument, Journal of Applied Polymer Science 131(22).
[26] D. Lee, (2018), Local anisotropy analysis based on the Mori-Tanaka model for multiphase composites with fiber length and orientation distributions, Composites Part B: Engineering 148 227-234.
[27] F.T. Fisher, L.C. Brinson, (2006), Nanomechanics of nanoreinforced polymers, Handbook of theoretical and computational nanoscience, American Scientific Publishers, pp. 253-360.
[28] T. Thorvaldsen, (2015), Modelling the elastic stiffness of nanocomposites using the Mori-Tanaka method.
[29] Y. Li, M. Zhou, (2013), Prediction of fracture toughness of ceramic composites as function of microstructure: I. Numerical simulations, Journal of the Mechanics and Physics of Solids 61(2) 472-488.
[30] B. Mortazavi, M. Baniassadi, J. Bardon, S. Ahzi, (2013), Modeling of two-phase random composite materials by finite element, Mori–Tanaka and strong contrast methods, Composites Part B: Engineering 45(1) 1117-1125.